Original Article

Evaluation of the microstructure, mechanical, and durability properties of alkali-activated slag-based mortar with light-burnt dolomite powder

In Kyu Jeon [a], Hong Gi Kim [b], Sadam Hussain Jakhrani [c], Jae-Suk Ryou [d,]*

[a] *Zachry Department of Civil & Environmental Engineering, Texas A&M University, College Station, TX, USA*
[b] *Civil & Environmental Engineering Department, Room 415, Jaesung Civil Engineering Building, 222 Wangsimni-ro, Seongdong Gu, Seoul, South Korea*
[c] *Civil Engineering Department, COMSATS University Islamabad (CUI), Sahiwal Campus, Sahiwal, 57000, Pakistan*
[d] *Civil & Environmental Engineering Department, Room 404, Jaesung Civil Engineering Building, 222 Wangsimni-ro, Seongdong Gu, Seoul, South Korea*

ARTICLE INFO

ABSTRACT

In this study, light-burnt dolomite powder was substituted for up to 20% of ground granulated blast-furnace slag in sodium sulfate-activated slag systems. The effects of light-burnt dolomite incorporation on compressive strength were investigated. Mineralogical analysis included XRD and FT-IR. Microstructure analysis included MIP and SEM examination. The durability properties, including carbonation depth and chloride penetration, were also investigated. The results indicate that the inclusion of LBD enhanced hydrotalcite and calcite formation and resulted in dense microstructures. All specimens with LBD had better mechanical and durability properties than did mixtures without LBD. Compared with 10% LBD incorporation, 20% LBD incorporation had fewer negative effects on mechanical and durability properties.

1. Introduction

Ordinary Portland cement (OPC) is commonly used as a raw material for construction worldwide. However, the cement manufacturing process produces large amounts of carbon dioxide and has severe impacts on the environment [1,2]. Approximately 5—8.6% of global carbon dioxide emissions are generated by the cement industry [3,4]. Thus, the replacement of OPC with various supplementary cementitious materials (SCMs) has been explored as a means to reduce carbon dioxide emissions.

Studies have investigated the use of SCMs through alkali activation to reduce OPC content and enhance the properties of OPC-based mixtures [5,6]. Alkali-activated material (AAM) is produced by a chemical reaction of aluminosilicate-based materials. The hydration characteristics of AAM are divided into three stages [7]. The first stage occurs in a high-alkaline environment with ionization of the aluminosilicate inside

raw materials, which is a decomposition–coagulation reaction. The second stage begins with a cumulative reaction process and enhances the number of precursors. The production of hydrated calcium aluminosilicate gel and hydrated calcium silicate gel occurs in the third stage, which is a condensation and crystallization reaction [8].

Ground granulated blast-furnace slag (GGBFS) and fly ash are common binder materials in AAM. In 1940, Prudon [9] discovered a method to use GGBFS as an aluminosilicate material to create an AAS mixture. The main hydration product of AAS is calcium aluminosilicate hydrate (C-A-S-H) gel, which has a different chemical structure than C–S–H gel due to the presence of penetrated Al^{3+} in tetrahedral bridging sites inside the C-A-S-H gel [10,11]. The incorporation of SCMs as a binder material in AAM is also attractive because most SCMs are selected from industrial by-products; thus, it is an effective approach to manage waste from an environmental perspective [12].

Dolomite ($CaMg(CO_3)_2$) can be obtained from natural sedimentary rock around the world; in addition, it is low cost and environmentally friendly [13]. Dolomite has a double carbonate of Ca and Mg and mainly consists of calcite and magnesite [14,15]. The calcined process of raw dolomite is important for enhancing its effectiveness. Calcined dolomite can be used as a source of magnesium in glass manufacturing and construction materials [14,16]. There are two parts to the thermal decomposition of dolomite [17,18]. The first part is the formation of calcite and magnesium oxide at lower temperatures (Eq. (1)). The second part occurs with increasing temperatures, which produces calcium oxide by disassembling calcite (Eq. (2)):

$$CaMg(CO_3)_2 \rightarrow CaCO_3 + MgO + CO_2 \qquad (1)$$

$$CaCO_3 \rightarrow CaO + CO_2 \qquad (2)$$
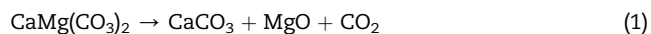
Light-burnt dolomite (LBD) can be obtained from raw dolomite through the calcination process between 900 and 1000 °C. LBD mainly consists of reactive MgO and CaO, which are alkaline earth activators [19,20]. Some previous studies have used calcined dolomite to improve the properties of cement composite. Jauffret et al. [21] studied half-burnt dolomite, which is calcined at 800 °C for 30 min as a replacement for OPC; the authors found that using 10–15 wt% half-burnt dolomite as an OPC replacement resulted in the greatest compressive strength. Yang et al. [22] studied light-burnt dolomite that was calcined at 900–1000 °C as an activator up to 2%; the authors found that compressive strength improved by 22–24% and delayed the initial setting time. Gu et al. [17] found that slag activated by calcined dolomite had higher sulfate resistance against sodium sulfate and magnesium sulfate than slag activated by OPC.

However, few studies have investigated the use of calcined dolomite as a binder material to replace GGBFS. Therefore, this study aims to investigate the effects of LBD used as a replacement for GGBFS on the microstructural, mechanical, and durability properties of alkali-activated slag-based mortar. LBD was used to replace 0%, 10%, and 20% of GGBFS, while OPC content was fixed at 10% and 20%. For this purpose, compressive strength, mercury intrusion porosimetry (MIP),

chloride penetration, carbonation, X-ray diffraction analysis (XRD), Fourier transform infrared spectroscopy (FT-IR), and scanning electron microscopy (SEM) were investigated.

2. Experimental

2.1. Materials

In this study, ordinary Portland cement (OPC) complying with ASTM C150 [23], ground granulated blast furnace slag (GGBFS), and light-burnt dolomite (LBD) were used as binder materials. LBD was produced by a local company in Gwangyang, Republic of Korea. Sodium sulfate anhydrous with a purity of 99% was used in this experiment as an activator. Table 1 shows the chemical composition and physical properties of OPC, GGBFS, and LBD, which were obtained by X-ray fluorescence (XRF, S8 Tiger). Fig. 1 represents the mineralogical composition of LBD obtained from XRD analysis. The XRD results indicate that LBD consisted of magnesium oxide, calcium oxide, calcium carbonate, and calcium hydroxide. Contrary to theoretical information, the existence of calcium hydroxide allows for the hydroxylation of calcium oxide by reacting with moisture from the ambient air [24]. Fig. 2 shows the particle size distributions of the binder materials, which were measured with a particle size analyzer (Malvern Mastersizer 2000). For the fine aggregate, natural sand with a maximum size of 5 mm, absorption of 1.05%, and fineness modulus (F.M) of 2.7 was used in this study.

2.2. Mix proportions and fabrication of specimens

Six mortar mixes were prepared in this study with a constant water-binder ratio of 0.4 and the same sand-binder ratio of 2. The mix proportions used to make the mortar mixes are shown in Table 2. Sodium sulfate with a purity of 99% used 4% (by weight) of binder as an alkali-activator in this study. OPC content was fixed at 10% and 20% in two mixture groups, which had three different LBD contents. LBD was replaced (by weight) with 0%, 10%, or 20% of cementitious binder materials in each mixture groups. The mortar mixes used in this study were given acronyms such as C10S90, C10S80L10, C10S70L20,

Table 1 – Chemical composition and physical properties of OPC, GGBFS, and LBD.

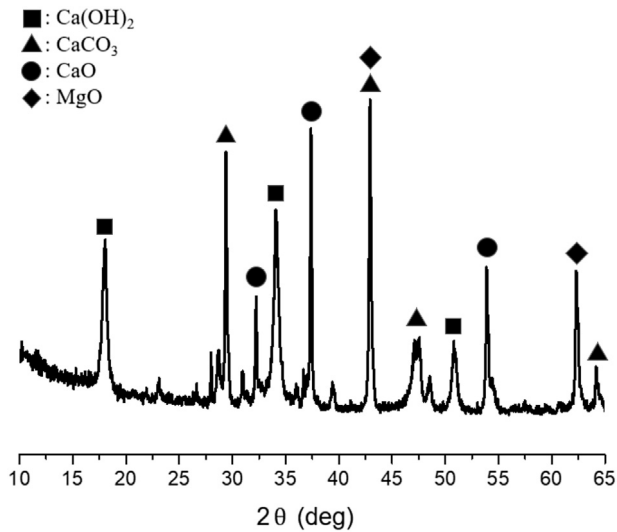| Composition	Weight (%)		
	OPC	GGBFS	LBD
SiO_2	20.8	34.1	3.0
Al_2O_3	6.3	16.1	1.3
Fe_2O_3	3.2	0.4	0.6
CaO	62	42.3	52.2
MgO	3.3	4.1	25.3
SO_3	2.2	2.5	0.4
Na_2O	–	–	0.06
K_2O	–	–	0.2
P_2O_5	–	–	0.03
TiO_2	–	–	–
Loss on ignition	1.3	0.05	1.85
Specific surface area [cm^2/g]	3200	4893	3038

Fig. 1 − **XRD patterns of LBD.**

C20S80, C20S70L10, and C20S60L20, in which C, S, and L indicate the contents of OPC, GGBFS, and LBD, in each mix.

Mortar cubes (50 × 50 × 50 mm³) were prepared in accordance with ASTM C109 [25]. Cylindrical specimens (Ø100 × 200 mm³) were prepared for chloride migration and carbonation tests. The mixes were cast in molds in three layers and were well compacted using a steel rod, as described in a previous study [26]. After mixing, the molds were vibrated for 30 s using a vibration table to remove any air voids. All molds were then sealed in plastic wrap to prevent moisture evaporation and stored in an ambient environment (20 ± 5 °C and 60 ± 5% RH) for 24 h. After 24 h, the mortar specimens were demolded and placed in lime-rich water at 23 ± 2 °C for further curing until the testing day.

2.3. Testing methods

The compressive strength tests were conducted using a universal testing machine (Shimadzu, CCM-200A; Shimadzu Corporation, Japan) after 3, 7, 28, 60, and 90 days of curing

followed by ASTM C109 [25]. For each test, three replicates were measured and the average value was recorded. To investigate the microstructure of AAS, mercury intrusion porosimetry was conducted using Micromeritics Autopore 9520 and a scanning electron microscope (accelerating voltage: 0.2—30 kV, probe current: 10E-12 to 10E-5A, SEI resolution: 3.5 nm, and magnification: 10 × to 300,000 ×) was used. For XRD and FT-IR analysis, powder samples were obtained from AAS specimens after 3 days and 7 days of curing using an X-ray diffractometer (RINT D/max 2500, 40 kV, 30 Ma, scanning speed 2°/min, wavelength 1.54 Å) and a spectrometer (Nicolet iS50, Thermo Fisher Scientific), respectively. In addition, a rapid chloride migration test (RMT) was conducted on mortar samples after 28 days of curing in accordance with NT BUILD 492 [27]; a carbonation test was measured using Ø100 × 50 mm obtained from cylindrical specimens. The cylindrical specimens for the carbonation test were sealed on all sides to allow the penetration of CO_2 from one surface. The specimens were placed in a laboratory carbonation chamber with 5% of CO_2 concentration at 20 °C and 60% relative humidity for 28 days. After 28 days in the CO_2 chamber, all specimens were split in half using a universal testing machine and the carbonation depth was measured by spraying phenolphthalein solution. The averages of at least ten measurements of depth were recorded for each specimen.

3. Results and discussion

3.1. Compressive strength

Fig. 3 shows the compressive strength of alkali-activated slag mortar with different LBD and OPC content after 3, 7, 28, 60, and 90 days of curing. The compressive strength values increased in all specimens as the curing age increased. The specimens also tended to exhibit slightly higher strength values in the group containing 20% OPC compared to the group containing 10% OPC. Variations in compressive strength due to the content of LBD showed that the incorporation of LBD resulted in higher strength regardless of the OPC content;
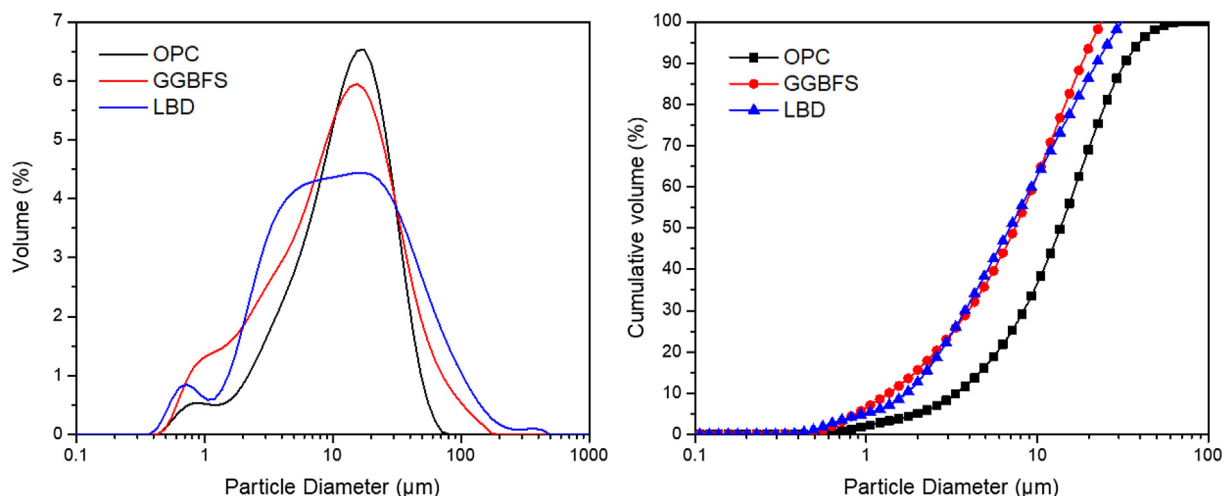

Fig. 2 − **Particle size distributions of OPC, GGBFS, and LBD.**

Table 2 – Mix proportions of alkali-activated slag mortar.

Mortar Mix	OPC (%)	GGBFS (%)	LBD (%)	Sodium sulfate (%)	Liquid/binder ratio	Sand/binder ratio
C10S90	10	90	0	4	0.4	2
C10S80L10	10	80	10	4	0.4	2
C10S70L20	10	70	20	4	0.4	2
C20S80	20	80	0	4	0.4	2
C20S70L10	20	70	10	4	0.4	2
C20S60L20	20	60	20	4	0.4	2

the highest strength was found in the 10% LBD mixtures. For example, C10S80L10 and C10S70L20 had values of 49.05 MPa and 44.15 MPa at 28 days of curing, which are 60% and 43.9% higher than those without LBD, respectively. In addition, C20S70L10 and C20S60L20 had values of 52.4% and 45.1% at 28 days of curing, which are 31.6% and 13.3% higher than that of C20S80, respectively. This could be demonstrated by the chemical properties of LBD. Machner et al. [28] attributed this enhancement of compressive strength to the carbonate addition of dolomite. The addition of carbonate in dolomite led to ettringite stabilization and produced the carbonate AFm phases. Yang et al. [22] found that LBD can accelerate the polymerization of an AAS system and consequently increase the compressive strength. However, previous researches [29–31] found that LBD mainly play a role as a filler in AAS system and replacement ratio of 20% has a little negative effect on the compressive strength development as agree with this experimental result. Lothenbach et al. [32] found that the incorporation of up to 40% dolomite can reduce the porosity by approximately 5%, thus accelerating the reaction process of slag due to a filler effect.

3.2. Mineralogy analysis

Fig. 4 shows the XRD mineralogy analysis of alkali-activated slag mortar at 3, 7, and 28 days. To investigate the minerals
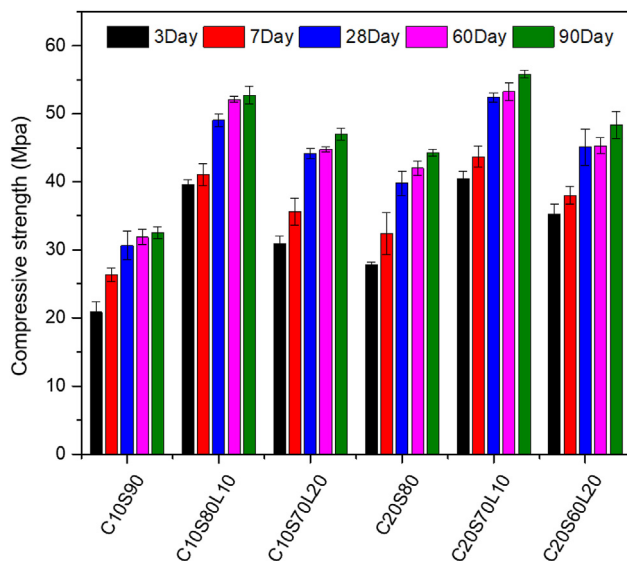
in the alkali-activated slag mortar generated by reactions with LBD replacement in the slag and OPC-based mixtures, OPC content was fixed at 10%. Fig. 4a shows the general XRD patterns of sodium sulfate-activated slag mixtures at 3, 7, and 28 days. Ettringite and C–S–H are known to be the major hydration products of slag mixtures activated with sodium sulfate [33]. Ettringite peak intensities were identified in all samples in Fig. 4a, regardless of curing days. Calcium hydroxide was also shown in all samples, unlike in normal sodium sulfate-activated slag mixtures, because of the OPC and GGBFS; however, its intensity decreased over the curing time. Gaylussite and calcite are the main carbonate salts in these sample; akermanite was identified due to the mineralogical properties of GGBFS. Hydrotalcite showed a slight increase in curing time but did not show much intensity overall. The distinct peak intensity of C/CSH, which represented the overlap of C–S–H and calcite, slightly increased with curing time.

Fig. 4b indicated the XRD patterns of C10S70L20, which has 20% LBD content, at 3, 7, and 28 days. Compared to Fig. 4a, b shows distinct peak intensities of hydrotalcite, calcite, gaylussite, and calcium hydroxide. In the case of hydrotalcite, all specimens showed peak intensities because a high amount of reactive MgO and CO_3^{2-} ions in LBD can react with Mg^{2+} and Al^{3+} obtained from GGBFS in a high-alkaline environment and promote the formation of hydrotalcite [34]. Moreover, gaylussite and calcite were observed in the pattern with high intensities due to the high amount of CO_3^{2-} in the LBD and the unavoidable carbonation of the hydration product. A previous study [34] found that the formation of hydrotalcite can accelerate the conversion of Ca^{2+} ions from gaylussite to a more stable state, such as the C-(A)-S-H phase. In Fig. 4a, the amount of gaylussite was shown to decrease as the amount of C–S–H increased over the curing time. However, Fig. 4b indicates that the amount of gaylussite and calcium hydroxide increased even when the amount of C–S–H increased, which is determined by the Ca^{2+} ions supplied from LBD and the effects of unsaturated GGBFS particles.

For the 0%, 10%, and 20% LBD included in the sodium sulfate-activated slag mixture (shown in Fig. 4c), the peak intensities of hydrotalcite, C–S–H, and calcite were enhanced with the content of LBD. This is because a high amount of reactive MgO in LBD can help to produce the hydrotalcite and calcite from CO_2^{-} in LBD.

Fig. 5 shows the FT-IR spectra (spectral range of 400–4000 cm^{-1}) of specimens. To investigate the impact of LBD on the alkali-activated slag system, 10% OPC mixes (C10S90, C10S80L10, and C10S70L20) at 3 days and 7 days of curing were used in this method. The sharp absorption peak
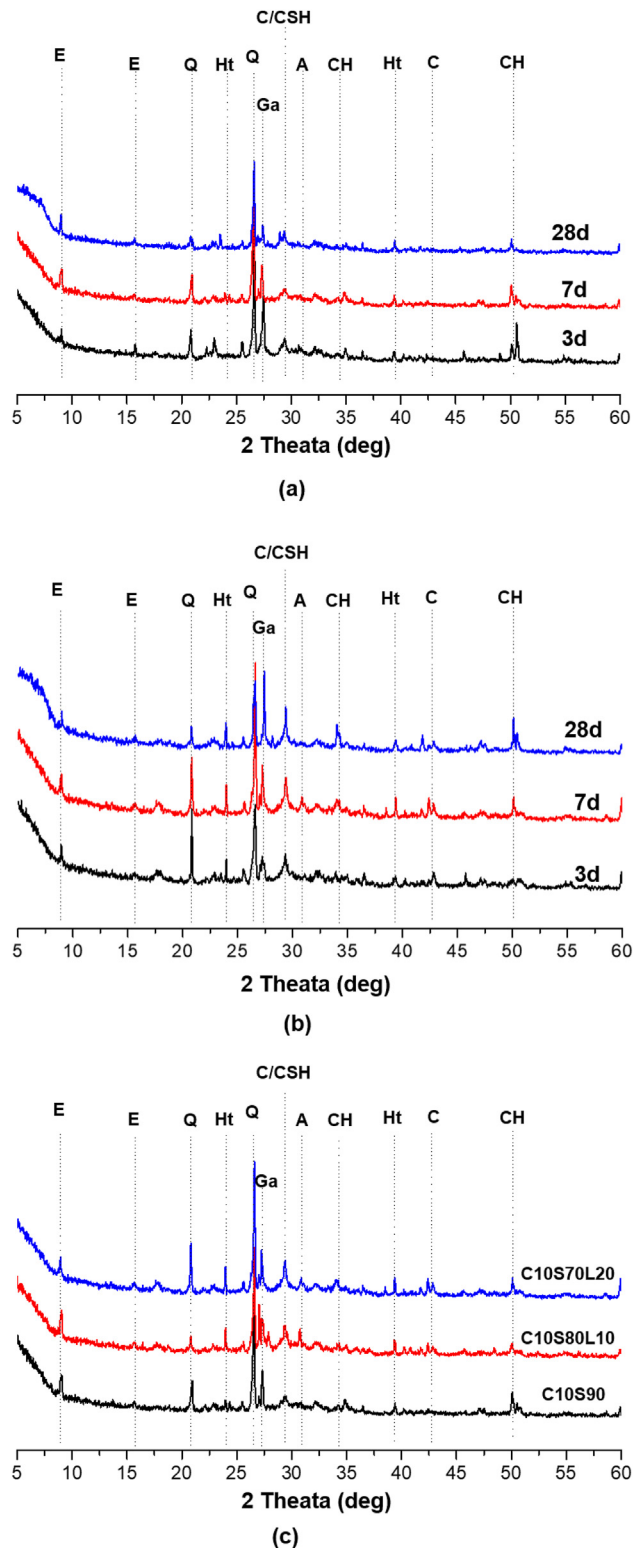

Fig. 3 – Compressive strength of alkali-activated slag mortars with different mixtures.

Fig. 4 − Mineralogical analysis of hydrated alkali-activated slag mortar at 3, 7, and 28 days for (a) C10S90, (b) C10S70L20, and (c) 10% OPC-based alkali-activated slag mortar with different LBD content at 7 day. Phases identified: E − ettringite $Ca_6Al_2(SO_4)_3(OH)_{12} \cdot 26H_2O$, Q − Quartz, Ht − hydrotalcite $Mg_6Al_2CO_3(OH)_{16} \cdot 4H_2O$, Ga − gaylussite $Na_2Ca(CO_3)_2 \cdot 5H_2O$, C − Calcite, CSH − Calcium silicate hydrate, A − akermanite $Ca_2Mg(Si_2O_7)$, CH − Calcium hydroxide.

was indicated in all specimens at different ages around 1002 cm^{-1}. In previous studies [35−38], this significant peak around 1002 cm^{-1} indicated the inhomogeneous stretching vibration of the Si−O bond of C-(A)-S-H gel, which is the main hydration product of alkali-activated slag composite; this is considered to be evidence of an alkali-activated polymerization process. Regardless of curing age, all specimens with LBD showed slightly higher peak intensity around 1002 cm^{-1}. LBD can accelerate the polymerization of alkali-activated slag composite, so a higher amount of hydration product was produced. Other distinct peaks at 1432 cm^{-1} and 1680 cm^{-1} can be attributed to the C−O stretching of the CO_3^{-2} [39]. The enhancement of these two peak intensities in specimens containing LBD may be due to the greater amount of calcite in LBD, which can produce more CO_3^{-2} inside the AAS system; in addition, a higher CaO dosage can increase the peak intensities [40]. The absorption peaks at 1650 cm^{-1} and 3100 to 3700 cm^{-1} indicate OH stretching vibrations in C−S−H, $Ca(OH)_2$, and chemically bound water [41]. It is difficult to conclude that the peaks of chemically bound water and hydration products overlap and result in only one effect. However, when comparing the results of the 3 days of curing with 7 days of curing, the effects of hydration products seems to be sufficient, indicating a marked increase in peak intensities. Higher peak intensities are shown for hydration products, such as C−S−H and $Ca(OH)_2$, with more curing time. In addition, higher peak values were found for the mixture containing LBD compared with the same curing period.

3.3. Microstructure analysis

Mercury intrusion porosimetry (MIP) experiments were conducted to obtain more information on the microstructure and hydration process, as shown in Figs. 6 and 7. To investigate the effect of LBD on the microstructure of an alkali-activated slag composite, C10S90, C10S80L10, and C10S70L20 were selected. According to previous research [42], pores can be classified as gel pores (interlayer C−S−H, <10 nm), capillary micropores (mesopores, 10−40 nm), or capillary macropores (40−10,000 nm). The effect of LBD on the pore size distribution of alkali-activated slag mortar at 28 days of curing are shown in Fig. 6. The results indicate that amount of gel pores increase with LBD content. The enhancement of gel pores is related to the number of C−S−H layers, as discussed in section 3.4 [43]. However, the micropore results showed that C10S80L10 and C10S90 specimens indicated similar amount, while C10S70L20 represented increased micropore than C10S90 and C10S890L10, which is contained 0% and 10% LBD. In addition, increment of micropore in 20% LBD specimen may affect the reduction of compressive strength result as mentioned in section 3.1.

Fig. 7 shows the total intrusion volume and total porosity of the alkali-activated slag system. A previous study [44] found that fine pore size distribution and a low porosity index lead to greater strength development; in addition, the shrinkage properties are related to the loss of water from the mesopores. The results indicate that the total intrusion volume was highest in specimens containing 0% LBD and was reduced at 20% and 10% LBD. The total porosity index of AAS system represented a trend like the intrusion volume. For
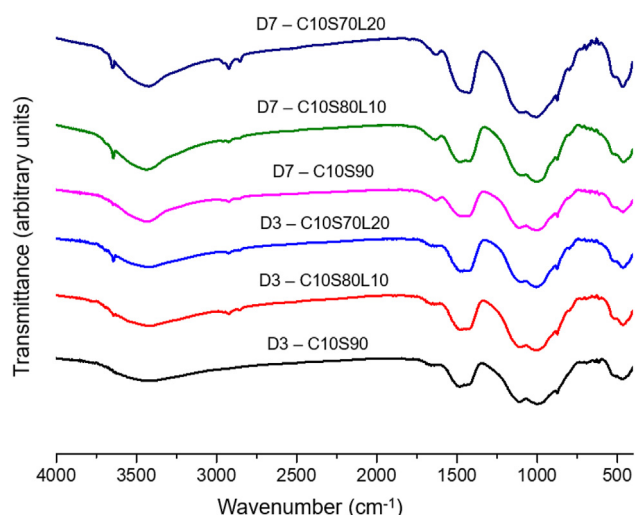
Fig. 5 – FTIR characterization of alkali-activated slag mortar with different LBD content and curing days.

example, the 10% LBD specimen (C10S80L10) showed 18.9%, which is a decrease of 10.4% compared to the specimen without LBD; the 20% LBD (C10S70L20) specimen indicated 19.1%, which was a decrease of 9.5% compared to the specimen without LBD, respectively. Although the highest gel pore volume was shown in the C10S70L20 specimen, the total porosity was the lowest in the C10S80L10 specimen due to the high micropore volume of C10S70L20; it is related to the compressive strength development, which agrees with the results obtained in a previous study [45].

Fig. 8 shows the SEM images of the fracture surfaces of sodium-sulfate activated slag after 7 days and 28 days of hydration. In Fig. 8a, needle-like ettringite, C–S–H, and unhydrated sodium sulfate are shown on the surface, which coincides with the previous sodium-sulfate activated slag composite. In addition, several capillary pores can be
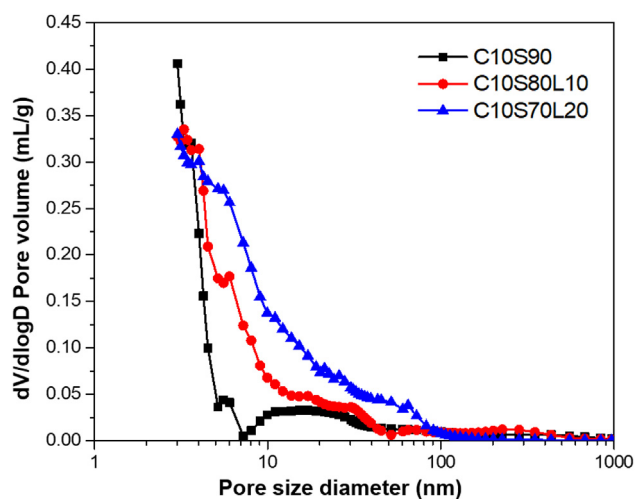

Fig. 6 – Pore size distribution of alkali-activated slag mortar with different LBD content at 28 days.

observed in Fig. 8a compared to Fig. 8b which represents the 20% LBD specimens at 7 days. Furthermore, calcium hydroxide and a hydrotalcite-like phase can be observed in Fig. 8b matrix, which is consistent with the results of the XRD results discussed in section 3.4. A large amount of C–S–H with calcium hydroxide, ettringite, and a hydrotalcite-like phase in Fig. 8b has a denser microstructure and contained fewer capillary pores in the matrix compared with Fig. 8a.

Fig. 8c and d shows the microstructures of sodium sulfate-activated slag mortar with and without LBD. Fig. 8c shows clear C–S–H gel forming a dense microstructure, with microcracks observe. However, in Fig. 8d, calcite can be observed clearly on the surface; the calcite is produced by the carbonate source in LBD. Encapsulated calcite in a C–S–H gel can lead a denser microstructure, which agrees with previous research [46].

3.4.   Carbonation test

The average carbonation depths of alkali-activated slag mortar with different LBD contents are shown in Fig. 9. Regardless of the OPC content in mixtures, all specimens showed a reduction in carbonation depths with LBD replacement. Carbonation depths of 17.37, 9.41, and 10.92 mm were measured for 10% OPC specimens with 0%, 10%, and 20% LBD, respectively. In addition, carbonation depths of approximately 12.34, 7.76, and 7.98 mm were measured for 20% OPC specimens with 0%, 10%, and 20% LBD. The replacement of LBD led to a decrease of 45.9% and 37.1% in 10% OPC mixtures and 37.1% and 35.33% in 20% OPC mixtures, respectively. Previous research [47] found that the carbonation resistance of cement composites, such as concrete, was mainly related to porosity—increasing with a reduction of porosity. This trend can be demonstrated by the pore size distribution and hydration products of alkali-activated slag mortar with LBD. Based on the MIP results, the inclusion of LBD can reduce the total intrusion volume and total porosity index. A large amount of hydration product in mixtures with LBD can lead to dense microstructures and thus high resistance to the penetration of CO_2 gas. Additionally, during the carbonation process, calcium hydroxide reacts with CO_2 to produce $CaCO_3$ and ettringite decomposes to form $CaCO_3$ due to CO_2 gas. However, the hydrotalcite-like phase shows resistance against carbonation, while other hydration products were decomposed by carbonation [48]. The carbonation depth has shown a tendency to increase slightly as the content of LBD increases from 10% to 20%, which can be explained by the micropore. More micropore were found in 20% LBD specimen and led to an increase in the total porosity and intrusion volume, which agrees with the MIP results.

3.5.   Rapid chloride migration test (RMT)

Fig. 10 shows the effect of LBD replacement on chloride penetration depth and the chloride migration coefficient of the studied alkali-activated slag mortars. A rapid chloride migration test was conducted according to NT build 492 [49] and the chloride migration coefficient was calculated by the following equation:
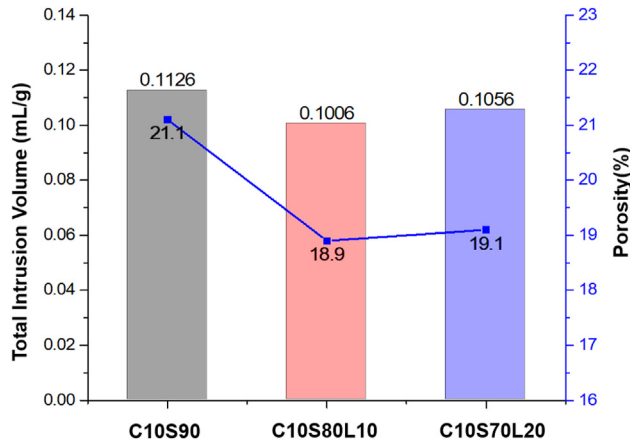
Fig. 7 − Total intrusion volume and total porosity of alkali-activated slag mortar.

Fig. 9 − Carbonation depths of the alkali-activated slag mortar specimens with different LBD content.

$$D_{nssm} = \frac{0.0239\,(273\,+\,T)L}{(U\,-\,2)t}\left(xd\,-\,0.0238\sqrt{\frac{(273\,+\,T)\,Lxd}{U\,-\,2}}\right)$$

Here, D_{nssm} is the chloride migration coefficient ($\times 10^{-12}$ m^2/s), T is average value of the initial and final temperatures in the anolyte solution (°C), L is the thickness of the specimen (mm), U is the absolute value of the applied voltage (V), x_d is the average value of the chloride penetration depths (mm), and t is the test duration (h).

The chloride penetration depth and migration coefficient results were similar to the carbonation results. In 10% OPC-based mixtures, C10S80L10 and C10S70L20 indicated 65.23%
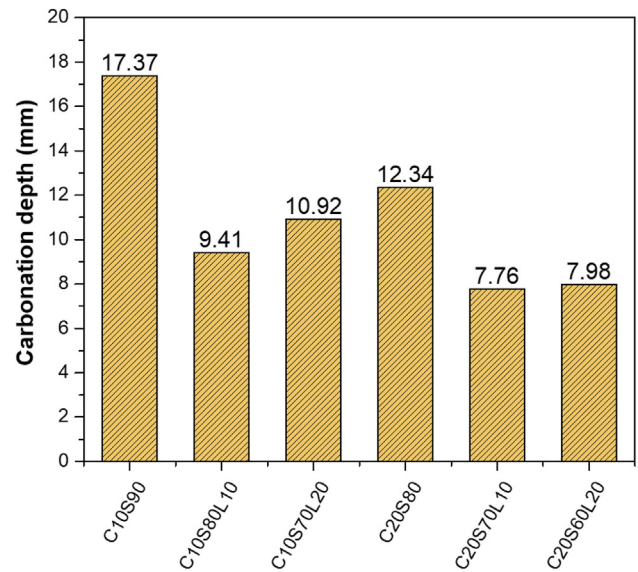
and 52.84% lower penetration depths than C10S90, respectively. Additionally, in 20% OPC-based mixtures, C20S70L10 and C20S60L20 showed 42.35% and 25.58% penetration depth reductions compared with C20S80, respectively. The observed enhancement may be due to the refinement of the microstructure through the replacement of LBD, which limited the penetration of chloride ions inside the alkali-activated slag mortar specimens. The improved microstructure of LBD-containing specimens due to the extra hydration product and calcite can be seen in Fig. 8. Additionally, Figs. 6 and 7
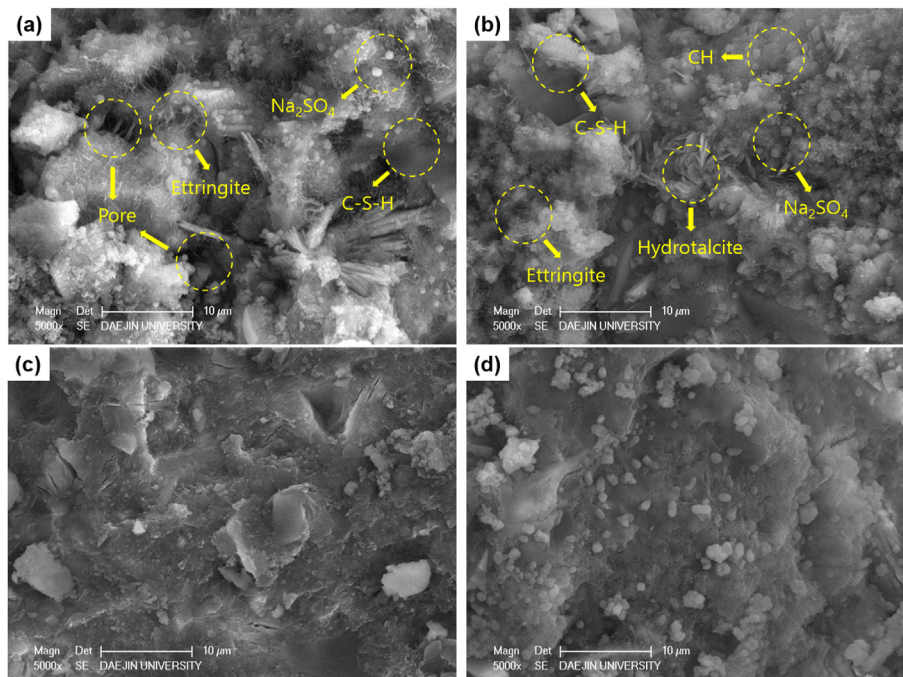

Fig. 8 − SEM images of (a) C10S90 at 7 days, (b) C10S70L20 at 7 days, (c) C10S90 at 28 days, and (d) C10S70L20 at 28 days.
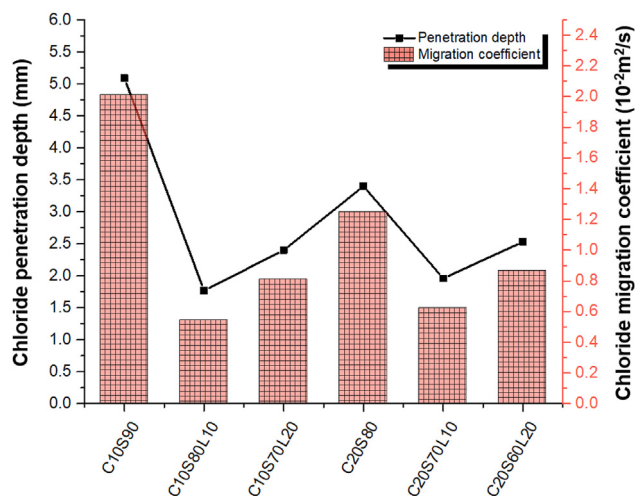
Fig. 10 — **Chloride penetration depths and chloride migration coefficients of alkali-activated slag mortar specimens with different LBD content.**

show increment of gel pores in composites due to more hydration product with LBD. However, 20% LBD mixtures had somewhat higher penetration depths and migration coefficients than did the 10% LBD mixtures due to the large amount of micropores inside the composite; this led to an increase in the total porosity index, which increased the permeability of chloride ions.

4. Conclusion

The influence of light-burnt dolomite powder on the microstructural, mechanical, and durability performance of alkali-activated slag-based mortar were investigated. The main findings can be summarized as follows:

1. The inclusion of LBD enhanced the compressive strength of alkali-activated slag-based mortar. In both 10% and 20% OPC mixtures, 10% LBD replacement had the highest compressive strength, which decreased slightly for 20% LBD replacement.
2. In the mineralogical analysis, LBD-containing mixtures had higher peak intensities for hydrotalcite, C—S—H, and calcite compared to mixtures without LBD due to the large amount of reactive CaO, MgO, and carbonate sources in LBD.
3. LBD replacement in mortar mixtures has positive filler effects, with more hydration product and thus denser microstructures. However, LBD replacement in excess of 10% can increase the micropores and enhance the total porosity index.
4. The carbonation depths of LBD-containing mortars were lower than that of mortars without LBD. Mixtures with 10% LBD had the lowest carbonation depths, with a slight increase for 20% LBD mixtures in both 10% and 20% OPC-based mortars. In addition, chloride penetration results showed similar tendencies as carbonation. Thus, the pore size distribution and microstructure affected the carbonation and chloride penetration results.

Availability of data and material

The datasets used and/or analyzed during the current study are available from the corresponding author on reasonable request.

Authors' contributions

In Kyu Jeon conceived, designed, and performed this experimental study under the guidance and supervision of Jae Suk Ryou and Hong Gi Kim. Sadam Hussain Jakhrani helped with writing the manuscript.

Funding

Declaration of Competing Interest

The authors declare that they have no competing interests.

REFERENCES

[1] McLellan BC, Williams RP, Lay J, Van Riessen A, Corder GD. Costs and carbon emissions for geopolymer pastes in comparison to ordinary portland cement. J Clean Prod 2011;19(9—10):1080—90.
[2] Habert G, Ouellet-Plamondon C. Recent update on the environmental impact of geopolymers. RILEM Tech Lett 2016;1:17—23.
[3] Worrell E, Price L, Martin N, Hendriks C, Meida LO. Carbon dioxide emissions from the global cement industry. Annu Rev Energy Environ 2001;26(1):303—29.
[4] Miller SA, Horvath A, Monteiro PJ. Readily implementable techniques can cut annual CO2 emissions from the production of concrete by over 20%. Environ Res Lett 2016;11(7):074029.
[5] Shi C, Roy D, Krivenko P. Alkali-activated cements and concretes. CRC press; 2003.
[6] Hu M, Zhu X, Long F. Alkali-activated fly ash-based geopolymers with zeolite or bentonite as additives. Cement Concr Compos 2009;31(10):762—8.
[7] Fernández-Jiménez A, Palomo A. Characterisation of fly ashes. Potential reactivity as alkaline cements☆. Fuel 2003;82(18):2259—65.
[8] Phoo-ngernkham T, Chindaprasirt P, Sata V, Hanjitsuwan S, Hatanaka S. The effect of adding nano-SiO2 and nano-Al2O3 on properties of high calcium fly ash geopolymer cured at ambient temperature. Mater Des 2014;55:58—65.
[9] Purdon A. The action of alkalis on blast-furnace slag. Journal of the Society of Chemical Industry 1940;59(9):191—202.
[10] Puertas F, Palacios M, Manzano H, Dolado J, Rico A, Rodríguez J. A model for the CASH gel formed in alkali-activated slag cements. J Eur Ceram Soc 2011;31(12):2043—56.

[11] Provis JL, Bernal SA. Geopolymers and related alkali-activated materials. Annu Rev Mater Res 2014;44:299—327.

[12] Part WK, Ramli M, Cheah CB. An overview on the influence of various factors on the properties of geopolymer concrete derived from industrial by-products. Construct Build Mater 2015;77:370—95.

[13] Ngamcharussrivichai C, Nunthasanti P, Tanachai S, Bunyakiat K. Biodiesel production through transesterification over natural calciums. Fuel Process Technol 2010;91(11):1409—15.

[14] Hossain F, Dlugogorski B, Kennedy E, Belova I, Murch G. First-principles study of the electronic, optical and bonding properties in dolomite. Comput Mater Sci 2011;50(3):1037—42.

[15] Ngamcharussrivichai C, Wiwatnimit W, Wangnoi S. Modified dolomites as catalysts for palm kernel oil transesterification. J Mol Catal A: Chem 2007;276(1—2):24—33.

[16] Olszak-Humienik M, Możejko J. Kinetics of thermal decomposition of dolomite. J Therm Anal Calorim 1999;56(2):829—33.

[17] Gu K, Jin F, Al-Tabbaa A, Shi B. Activation of ground granulated blast furnace slag by using calcined dolomite. Construct Build Mater 2014;68:252—8.

[18] Maitra S, Choudhury A, Das H, Pramanik MJ. Effect of compaction on the kinetics of thermal decomposition of dolomite under non-isothermal condition. J Mater Sci 2005;40(18):4749—51.

[19] Kim MS, Jun Y, Lee C, Oh JE. Use of CaO as an activator for producing a price-competitive non-cement structural binder using ground granulated blast furnace slag. Cement Concr Res 2013;54:208—14.

[20] Jin F, Gu K, Al-Tabbaa A. Strength and hydration properties of reactive MgO-activated ground granulated blastfurnace slag paste. Cement Concr Compos 2015;57:8—16.

[21] Jauffret G, Glasser FP. Thermally activated dolomite as pozzolanic addition to Portland cement. Adv Cement Res 2016;28(6):378—88.

[22] Yang W-H, Ryu D-W, Park D-C, Kim W-J, Seo C-H. A study of the effect of light-burnt dolomite on the hydration of alkali-activated Portland blast-furnace slag cement. Construct Build Mater 2014;57:24—9.

[23] ASTM. ASTM C150/C150M-12: standard specification for Portland cement. Conshohocken, PA, USA: ASTM International West; 2012.

[24] Caceres P, Attiogbe E. Thermal decomposition of dolomite and the extraction of its constituents. Miner Eng 1997;10(10):1165—76.

[25] A. ASTM. Standard test method for compressive strength of hydraulic cement mortars (using 2-in. or [50-mm] cube specimens). 1. In: Annual Book of ASTM StandardsAnnual Book of ASTM Standards. 4; 2013. p. 1—9.

[26] Qudoos A, Kim HG, Jeon IK, Ryou J-S. Influence of the particle size of wheat straw ash on the microstructure of the interfacial transition zone. Powder Technol 2019;352:453—61.

[27] N. Nordtest, BUILD 492. Chloride migration coefficient from non-steady-state migration experiments. Finland: Nordtest; 1999.

[28] Machner A, Zajac M, Haha MB, Kjellsen KO, Geiker MR, De Weerdt K. Portland metakaolin cement containing dolomite or limestone—Similarities and differences in phase assemblage and compressive strength. Construct Build Mater 2017;157:214—25.

[29] Ye H, Fu C, Yang G. Influence of dolomite on the properties and microstructure of alkali-activated slag with and without pulverized fly ash. Cement Concr Compos 2019;103:224—32.

[30] Ye H, Fu C, Yang G. Alkali-activated slag substituted by metakaolin and dolomite at 20 and 50° C. Cement Concr Compos 2020;105:103442.

[31] Jeon IK, Ryou JS, Jakhrani SH, Kim HG. Effects of light-burnt dolomite incorporation on the setting, strength, and drying

[31] shrinkage of one-Part Alkali-activated slag cement. Materials 2019;12(18):2874.

[32] Lothenbach B, Scrivener K, Hooton R. Supplementary cementitious materials. Cement Concr Res 2011;41(12):1244—56.

[33] Rashad A, Bai Y, Basheer P, Milestone N, Collier N. Hydration and properties of sodium sulfate activated slag. Cement Concr Compos 2013;37:20—9.

[34] Bernal SA, Provis JL, Myers RJ, San Nicolas R, van Deventer JS. Role of carbonates in the chemical evolution of sodium carbonate-activated slag binders. Mater Struct 2015;48(3):517—29.

[35] Garcia-Lodeiro I, Palomo A, Fernández-Jiménez A, Macphee D. Compatibility studies between NASH and CASH gels. Study in the ternary diagram Na2O—CaO—Al2O3—SiO2—H2O. Cement Concr Res 2011;41(9):923—31.

[36] Phair J, Van Deventer J. Effect of the silicate activator pH on the microstructural characteristics of waste-based geopolymers. Int J Miner Process 2002;66(1—4):121—43.

[37] Gadsden J. In: Infrared spectra of minerals and related inorganic compounds, vol. 220. London, UK: Buttherworth; 1975. p. 221.

[38] Rees CA, Provis JL, Lukey GC, van Deventer JS. Attenuated total reflectance fourier transform infrared analysis of fly ash geopolymer gel aging. Langmuir 2007;23(15):8170—9.

[39] Fernández-Carrasco L, Torrens-Martín D, Morales L, Martínez-Ramírez S. Infrared spectroscopy in the analysis of building and construction materials, Infrared spectroscopy—materials science, engineering and technology. INTECH; 2012. p. 369—82.

[40] He J, Yang C-h. Influence of carbonation on microstructure of alkali-activated slag cement pastes. J Build Mater 2012;1.

[41] Yu P, Kirkpatrick RJ, Poe B, McMillan PF, Cong X. Structure of calcium silicate hydrate (C-S-H): near-, mid-, and far-infrared spectroscopy. J Am Ceram Soc 1999;82(3):742—8.

[42] Najimi M, Ghafoori N. Engineering properties of natural pozzolan/slag based alkali-activated concrete. Construct Build Mater 2019;208:46—62.

[43] Gao P, Ye G, Wei J, Yu Q. Multi-scale simulation of capillary pores and gel pores in Portland cement paste. In: 14th international congress on the chemistry of cement (ICCC 2015); 2015. p. 1—14.

[44] Collins F, Sanjayan JG. Effect of pore size distribution on drying shrinking of alkali-activated slag concrete. Cement Concr Res 2000;30(9):1401—6.

[45] Shi C, Tang X, Li Y. Studies on the activation of phosphorus slag. In: Proceedings of the third international conference on the use of fly ash. Silica Fume, Slag and Natural Pozzolans in Concrete; 1989. p. 657—66.

[46] Tan H, Deng X, He X, Zhang J, Zhang X, Su Y, et al. Compressive strength and hydration process of wet-grinded granulated blast-furnace slag activated by sodium sulfate and sodium carbonate. Cement Concr Compos 2019;97:387—98.

[47] Gonen T, Yazicioglu S. The influence of compaction pores on sorptivity and carbonation of concrete. Construct Build Mater 2007;21(5):1040—5.

[48] Machner A, Zajac M, Haha MB, Kjellsen KO, Geiker MR, De Weerdt K. Stability of the hydrate phase assemblage in Portland composite cements containing dolomite and metakaolin after leaching, carbonation, and chloride exposure. Cement Concr Compos 2018;89:89—106.

[49] N. Build, 492. In: Concrete, mortar and cement-based repair materials: chloride migration coefficient from non-steady-state migration experiments, vol. 3; 1999.